Turbulent Times in the Northern Polar Ionosphere?

Robert Burston, Ivan Astin, Cathryn Mitchell, University of Bath, UK.

Lucilla Alfonsi, Istituto Nazionale di Geofisica e Vulcanologia,

Rome.

Todd Pedersen, Space Vehicles Directorate, Air Force Research

Laboratory, Hanscom AFB, MA, USA

Susan Skone, Department of Geomatics Engineering, Schulich School of Engineering,

University of Calgary, Canada.

Abstract

A model is presented of the growth rate of turbulently generated irregularities in the electron concentration of northern polar cap plasma patches. The turbulence is generated by the short-term fluctuations in the electric field imposed on the polar-cap ionosphere by electric field mapping from the magnetosphere. The model uses an ionospheric imaging algorithm to specify the state of the ionosphere, throughout. The growth rates are used to estimate mean amplitudes for the irregularities and these mean amplitudes are compared with observations of the scintillation indices, S_4 and σ_ϕ, by calculating the linear correlation co-efficients between them. The scintillation data are recorded by GPS L1 band receivers stationed at high northern latitudes. A total of 13 days are analysed, covering four separate magnetic storm periods. These results are compared with those from a similar model of the Gradient Drift Instability (GDI) growth rate. Over-all, the results show better correlation between the GDI process and the scintillation indices than for the turbulence process and the scintillation indices. Two storms, however, show approximately equally good

correlations for both processes, indicating that there might be times when the turbulence process of irregularity formation on plasma patches may be the controlling one.

Introduction

Plasma patches, amorphous "islands" of high electron concentration, observed most frequently in the winter night-time polar cap ionosphere [*Hunsucker*, 2003], are associated with scintillation of Global Positioning System (GPS) L1 band radio signals [*Chaturvedi et al.*, 1994; *Coley and Heelis*, 1995; *Gondarenko and Guzdar*, 1999; 2001; *Gondarenko et al.*, 2003; *Gondarenko and Guzdar*, 2004a; b; *Gondarenko et al.*, 2005; *Gondarenko*, 2006a; b; *Kersley et al.*, 1989; *Kivanc and Heelis*, 1997; *Sojka et al.*, 1998]. Such patches are 100s to 1000s of kilometres in scale and appear only when the Interplanetary Magnetic Field points southward and the geo-magnetic field is disturbed [*Hunsucker*, 2003]. See fig.1. Ionospheric scintillation is the phenomenon of unwanted random variations in the intensity and/or phase of a radio signal, introduced to the signal as it traverses the ionosphere [*Hargreaves*, 1992]. Such scintillations can negatively impact on navigation and aircraft landing systems that rely on GPS [*Kaplan*, 1996]. Understanding the causes of GPS L1 band scintillation is therefore of practical as well as scientific interest.

In general, ionospheric scintillation is understood to be generated when a radio signal passes through a region of the ionosphere containing "irregularities." Irregularities are fluctuations in electron concentration that cause the Refractive Index of the ionosphere to change significantly within the space of several wavelengths of

the transmitted signal [*Davies*, 1990]. These irregularities cause the signal to be refracted in an unpredictable manner at different points along the wave-front. The random phase changes introduced to the signal by this process are phase-scintillations. Amplitude scintillations develop as the phase changes cause wave interference along the wave-front as it continues to propagate. Irregularities can exist on all scales from metres to thousands of metres. For any given radio frequency and satellite-ionosphere-receiver geometry there is a scale size above which irregularities will not cause amplitude scintillation. This can be estimated using the concept of the First Fresnel Zone [*Hargreaves*, 1992; *Hunsucker*, 2003].

Ionospheric scintillation is most commonly measured by two indices, S_4 and σ_ϕ. S_4 is a measure of amplitude fading and is defined as

$$S_4 = \frac{\sqrt{\left\langle \left(P - \langle P \rangle \right)^2 \right\rangle}}{\langle P \rangle} \tag{1.1}$$

where P is the received power and the symbols $\langle\rangle$ imply the mean value.

σ_ϕ is a measure of phase scintillation, defined as

$$\sigma_\phi^2 = \left\langle \phi^2 \right\rangle - \left\langle \phi \right\rangle^2, \tag{1.2}$$

where ϕ is the measured phase. Again, $\langle\rangle$ implies the mean value [*Hargreaves*, 1992; *Hunsucker*, 2003].

Two mechanisms of irregularity formation in plasma patches have been proposed. The most thoroughly studied is the Gradient Drift Instability (GDI) [*Chaturvedi et al.*, 1994; *Coley and Heelis*, 1995; *Gondarenko and Guzdar*, 1999;

2001; *Gondarenko et al.*, 2003; *Gondarenko and Guzdar*, 2004a; b; *Gondarenko et al.*, 2005; *Gondarenko*, 2006a; b; *Kersley et al.*, 1989; *Kivanc and Heelis*, 1997; *Sojka et al.*, 1998]. This is a plasma instability that can occur when an electric field, a magnetic field and a gradient in electron concentration are all present and mutually perpendicular to each other. In the polar cap, the Earth's magnetic field is almost vertical. Electric fields with significant horizontal components can be mapped to the polar cap ionosphere from the magnetosphere. The edges of plasma patches have steep gradients in electron concentration so all the requirements for the GDI to occur can be fulfilled. By definition, a plasma instability is a wave that grows in amplitude exponentially with time. The exponent is defined as a growth-rate, γ [*Kelley*, 1989]. The linear growth-rate for the GDI is given by

$$\gamma_{GD} = \frac{\mathbf{E}\times\mathbf{B}}{B^2}\cdot\left(\frac{\nabla n_0}{n_0}\right) \tag{1.3}$$

(collisional plasma) or

$$\gamma_{GD} = \left[\upsilon_{in}\left(\frac{\mathbf{E}\times\mathbf{B}}{B^2}\right)\cdot\left(\frac{\nabla n_0}{n_0}\right)\right]^{1/2} \tag{1.4}$$

(collisionless/inertial plasma), where n_0 is the electron concentration, **E** is the electric field strength, **B** is the magnetic field strength and υ_{in} is the ion-neutral collision frequency [*Sojka et al.*, 1998]. The Current Convective Instability is a plasma instability that allows formation of Gradient Drift Waves on otherwise stable plasma concentration gradients if there is a sufficient field-aligned current present and a component of the initial perturbing wave is parallel to **E** [*Chaturvedi and Ossakow*, 1979; 1981; *Huba*, 1984; *Ossakow and Chaturvedi*, 1979]. Conditions required for the CCI are rarely met and hence it mentioned here only for completeness [*Kelley*, 1989].

The other mechanism proposed in the literature is a turbulence process and has not received as much attention as the GDI [*H. Mounir*, 1991; *Huba et al.*, 1985; *Kintner and Seyler*, 1985; *Kunitsyn and Tereshchenko*, 1992; *Mounir et al.*, 1991; *Zvezdin and Fridman*, 1992]. Electric fields of magnetospheric origin are mapped to the polar cap ionosphere along the Earth's magnetic field. The quasi-d.c. (i.e. varying over time-scales of many minutes or longer) components of these electric fields drive **ExB** drifts of plasma in the polar caps, in a large scale circulation pattern. Plasma patches can travel for several hours following this circulation pattern before they lose their identity [*Hargreaves*, 1992; *Kelley*, 1989].

The magnetospheric electric fields are "turbulent" in that they show continual variation at short timescales and these fluctuations are also mapped to the ionosphere, exposing plasma to rapidly varying **ExB** drifts that can cause Gradient Drift Instabilities, generating turbulent mixing of the plasma, if there is an electron-concentration gradient present [*Kelley*, 1989].

[*Kelley*, 1989] develops a growth-rate, γ_T, for this turbulence process that can be directly compared to γ_{GD}:

$$\gamma_T = \frac{\left[\int_{k_L}^{\infty} E(k)^2 dk\right]^{1/2} . |\nabla n_0|}{B n_0}, \qquad (1.5)$$

where k_L, the shortest relevant wavenumber is defined as $k_L = 2\pi \frac{|\nabla n_0|}{n_0}$, k is the wavenumber and $E(k)$ is the electric field as a function of wavenumber. A non-

vector equation is used as it is assumed that the fluctuations of the electric field are random in direction and therefore some part of the patch is unstable to any given one. The fluctuations are suggested to be of the order of E_0, the quasi-d.c. value of the electric field, in (ref Kelley 2009) and this is assumed to be the case for the purposes of the model presented in this paper.

In this paper a model of γ_T is developed, utilising a 4-dimensional ionospheric imaging algorithm (MIDAS 2.0 [*Spencer and Mitchell*, 2007]) to specify the state of the ionosphere in terms of n_0 and utilising the Weimer Model to specify the plasma drift velocity at all times and locations under study. The growth-rate values are in turn used to calculate irregularity wave amplitudes.

Observations of the scintillation indices S_4 and σ_ϕ are separately correlated with mean wave amplitude values for a number of magnetic storm periods. The linear correlation co-efficients are presented and compared with the equivalent results from a similar model of the GDI process [*Burston et al.*, 2009]. The results of that paper are shown in figs.4-14 (part a of each). The primary conclusion of the paper is that weak but significant correlation exists between the model implemented and the observations of the scintillation indices, S_4 and σ_ϕ when geomagnetic storm conditions apply to the northern polar-cap ionosphere.

Method

The analysis presented here follows [*Burston et al.*, 2009] in its method as far as is possible in order to make direct comparison of the results possible. It only differs in that in the previous work the GDI was modelled using equation (1.4) where-as here turbulence is modelled using equation (1.5). Full details of the method are presented again here for ease of understanding.

The spatial grid used by MIDAS 2.0 is divided into voxels by latitude, longitude and altitude surfaces. Because of the curvature of the earth, the resulting grid voxels are not of equal size. In this work an altitude interval of 40km is used. The total altitude range is 140km to 1660km. In order to discover the optimum latitude/longitude divisions, a number of grids were defined, then the algorithm was run for each, using the same input data and time period: 09.00 UT, Oct 30th to 12.00 UT Oct 31st, 2003, inclusive. Ten minute time intervals between each reconstruction were used in all cases. All other parameters in the algorithm were set identically in each case. The resulting TEC map images were compared with independently supplied all-sky camera images for the same time period. The all-sky camera is stationed in Qaanaaq Greenland (76º, 32’ lat. / 68º, 50’ long.)

The latitude/longitude grid separations tested in this way were the 16 possible combinations of integer values 2 through 5, in degrees. The two combinations that gave TEC map images most similar to the all-sky camera images were 4º x 4º and 4º x 2º, latitude x longitude. Because the latter combination gives better resolution (i.e. a greater total number of voxels in the grid) whilst giving equally good results, a 4º x

2º, latitude x longitude grid definition was chosen for use in the model of the turbulence growth rate (see fig.2). Having defined the optimum grid, MIDAS 2.0 was used to produce reconstructions of the ionosphere for a number of geo-magnetic storm periods, as detailed in table 1. Ten minute intervals between individual images were used through-out.

Values of γ_T were subsequently calculated for each voxel of each reconstruction, by using equation (1.5). Linear theory is used because, as with the GDI model of [*Burston et al.*, 2009], the non-linear correction is small compared to the error in the growth rate caused by the calculation of the electron concentration gradient from the relatively coarse grid used by the imaging algorithm. The magnetic field strength B is obtained from the IGRF model. The IGRF model is a model of the Earth's magnetic field requiring only spatial co-ordinates and a date as inputs and giving the magnetic field strength as output. The model extends beyond ionospheric altitudes so results for all grid voxels and times can be obtained [*Macmillan and Maus*, 2005; *Maus et al.*, 2005a; b; *Maus et al.*, 2005c]. $\frac{\nabla n_0}{n_0}$ is calculated directly from the MIDAS 2.0 results. E(k) is needed to perform the integral, however, and this is difficult to obtain: There are few published electric field spectra so the ideal case of specifying E(k) at all times and locations from directly observed data is impossible. Some assumption about the nature of E(k) must be made in order to progress.

[*Mounir et al.*, 1991] used ARCAD-AUREOL-3 observations to obtain values of the electric field. (The ARCAD-AUREOL-3 satellite had a polar orbit and

instruments for measuring the in-situ electric field as two perpendicular components, one being in the local horizontal plane.) The measurements of this component of the electric field from several orbits were used to obtain power spectral density graphs. Linear least squares fits to the data (plotted as log-log graphs) were obtained and the slopes of the resulting straight lines calculated. Slopes obtained in such a manner are referred to as the "spectral indices" of the graphs. A bar-chart of the occurrence of the spectral indices is also presented by [*Mounir et al.*, 1991]. The most frequently occurring spectral indices were in the range 1.6 to 1.8. These data allow a calculation to be made that gives values for the integral,

$$\int_{k_L}^{\infty} E(k)^2 dk . \tag{1.6}$$

The data presented in this paper are all that could be obtained that allow equation (1.6) to be solved. They are not ideal as the fading frequency range for a GPS L1 band signal cannot be expected to be identical to that shown in [*Mounir et al.*, 1991] for the ARCAD-AUREOL-3 satellite. This introduces a source of error into the value of the spectral index that is not readily quantifiable.

From fig.3 it can be seen that

$$\log(E(k)^2) = -\rho \log(k) + \log(\beta) \tag{1.7}$$

or

$$E(k)^2 = \beta k^{-\rho} \tag{1.8}$$

where ρ = the modulus of the spectral index (the minus sign is present because the slope is always negative) and β = a constant obtained from the graph by evaluating $\beta = C.10^{-\rho}$.

Substituting equation (1.8) into equation (1.6) gives

$$\int_{k_L}^{\infty} E(k)^2 dk = \int_{k_L}^{\infty} \beta k^{-\rho} dk \Rightarrow \beta \left[\frac{k^{1-\rho}}{1-\rho} \right]_{K_L}^{\infty} \tag{1.9}$$

$$\Rightarrow 0 - \beta k_L^{1-\rho} / (1-\rho) = \beta k_L^{1-\rho} / (\rho - 1). \tag{1.10}$$

To progress from here, the expression for k_L and values for the constants ρ and β must be substituted into equation (1.10). The value 1.6 was selected for ρ as it is in the range of most frequently occurring values according to the bar chart presented by [*Mounir et al.*, 1991] and the range 1.4 to 1.6 occurs much more frequently than the range 1.8 to 2.0. ([*Kelley*, 2009] notes that the spectral index expected for the GDI process is nearly 2.5.) Only one graph of the power spectral density is presented by [*Mounir et al.*, 1991] so there is little choice but to calculate β directly from it: $\beta = 4.27 \text{x} 10^{-5}$ (see fig.5). Making these substitutions gives

$$\int_{k_L}^{\infty} E(k)^2 dk = \frac{4.27 \text{x} 10^{-5} . \left[2\pi . (\nabla n_e / n_e) \right]^{-0.6}}{0.6}. \tag{1.11}$$

Substituting this into equation (1.5) for γ_T yields

$$\gamma_T = \left(\frac{4.27 \text{x} 10^{-5} . \left[2\pi . (\nabla n_e / n_e) \right]^{-0.6}}{0.6} \right)^{1/2} . \left(\frac{\nabla n_e}{n_e B} \right), \tag{1.12}$$

and simplifying slightly:

$$\gamma_T = \left(\frac{4.27 \text{x} 10^{-5}}{0.6} \right)^{1/2} . \left[2\pi . (\nabla n_e / n_e) \right]^{-0.3} . \left(\frac{\nabla n_e}{n_e B} \right). \tag{1.13}$$

Equation (1.13) is the turbulence growth rate required for the model used in this analysis. This type of model of the effects of turbulence has not been presented in the literature previously.

Scintillation observations were recorded by GSV4004 GPS receivers. These receivers record data at a rate of 50Hz and subsequently calculate statistical data at 1 minute intervals. The receivers used in this and subsequent studies are stationed as shown in table 2 and fig.4. Data were not available from all stations on all days.

Scintillation observations from the receivers come in the form of S_4 and σ_ϕ values. The σ_ϕ values are available over the mean times of 1, 3, 10, 30 and 60 seconds. The elevation and azimuth of all GPS satellites detected by the receiver is also recorded and given as part of the 1 minute data. This information can be used to calculate the position of the ionospheric pierce point (IPP) of all received signals, if an arbitrary altitude for the pierce point is selected. (The ionospheric pierce point is the point where a signal ray intersects with the ionosphere. The ionosphere is assumed to be an infinitely thin layer at a specific altitude for this purpose.) These IPPs were mapped to the nearest voxel in the MIDAS 2.0 grids. Since the MIDAS 2.0 grid is updated only every ten minutes but scintillation data, including elevation and azimuth of satellites, is updated every minute, it is possible that multiple observations exist mapped to the same grid voxel during the same ten minutes.

The growth rate, γ_T, can take on positive, negative or zero values and in general will vary through time. The amplitude of the actual waves, will vary accordingly, however, it can only be positive or zero. Since the waves are the cause of the variations in electron concentration that ultimately cause a radio wave to scintillate, it is the amplitudes of these waves that are of true interest. Computing a correlation co-efficient between the observed scintillation indices and the

instantaneous growth rate at the voxel containing the ionospheric pierce point of the observation, at the time of the observation is straight-forward. This does not give an indication of the wave amplitude at that time and location, though. It would be useful to have knowledge of how the plasma has been affected by the turbulence through time as

$$\mathrm{A} \propto e^{\gamma t} \tag{1.14}$$

by definition. (A is the amplitude of an unstable wave, t is time, γ is the growth rate.) If the value of γ_{T} is known from t = 0 to t = time of scintillation observation, then it would be possible to calculate a mean amplitude for a wave over the same time interval, as follows:

Assume that there is a series of known values of γ_{T}, each assumed to be constant for ten minutes. The mean amplitude is then given by,

$$\overline{\mathrm{A}} = \left(\int_0^t \mathrm{E}_0 e^{\gamma t} dt - \mathrm{E}_0 t \right) / t \tag{1.15}$$

where $\overline{\mathrm{A}}$ is the mean amplitude, E_0 is the initial (unperturbed) electric field value, t is the total time elapsed and $\gamma = \sum_j \gamma_j$, γ_j being the jth turbulence growth rate in the series.

This can by evaluated analytically:

$$\int_0^t \mathrm{E}_0 e^{\gamma t} dt = \left[\mathrm{E}_0 e^{\gamma t} / \gamma \right]_0^t = \left(\mathrm{E}_0 / \gamma \right) \left(e^{\gamma t} - 1 \right) \tag{1.16}$$

and, if γt is small, $e^{\gamma t} \approx 1 + \gamma t + \left(\frac{\gamma^2 t^2}{2!} \right)$, hence $e^{\gamma t} - 1 = \gamma t + \left(\frac{\gamma^2 t^2}{2!} \right)$

$$\therefore \qquad \overline{\mathrm{A}} = \frac{\left(\frac{E_0}{\gamma}\right)\left[\gamma t + \left(\frac{\gamma^2 t^2}{2!}\right)\right] - E_0 t}{t}. \qquad (1.17)$$

Equation (1.17) simplifies to:

$$\overline{\mathrm{A}} = \frac{\mathrm{E}_0 \gamma t}{2}. \qquad (1.18)$$

Obtaining a series of values for γ_T is possible because MIDAS 2.0 provides values for the plasma drift velocity, as computed by the Weimer Model, and updated every ten minutes along with the electron concentration values. Converting the velocities to units of voxels per second and ignoring possible vertical motion, it is possible to trace the motion of a plasma packet back through time, to an accuracy of the nearest voxel. As values of γ_T are calculated for all voxels at all times, the series of values at ten minutes intervals can be found and used in equation (1.18). A correlation co-efficient can then be calculated for all observations and their associated mean amplitude values.

Analyses were conducted on a daily basis, with the first MIDAS 2.0 output at 00.00 UT and the last at 23.50 UT of the same day. This means that for the first output grid, only the instantaneous growth rate is known. For the last, potentially 24 hours of history is known. It is possible that the Weimer drift velocity indicates that a plasma packet has left the voxel grid entirely. In such circumstances, a hole would appear in the grid, so it is assumed that a new plasma packet replaces it, with a new series of γ_T starting from t = 0 at the time of appearance of the new packet. Because a plasma packet could appear at any time it is, in general, not possible to predict the length of time that the mean amplitude must be calculated over and mean amplitudes will have been calculated over various lengths of time between ten minutes and 24

hours. The amplitude of the wave is arbitrarily assumed to be zero at the start of the available time series. This means that initial values of the growth rate equal to or less than zero have no impact and can be ignored, as can every such value that comes before the first positive value.

When multiple scintillation observations have IPPs occurring in the same voxel in the same ten minute time interval, mean values of the scintillation indices are calculated and used subsequently for the calculation of the correlation co-efficients.

Since the choice of ionospheric altitude is crucial but arbitrary in this analysis, it was repeated for every altitude step in the voxel grid.

Results

Table 3 shows which scintillation receiver stations' data were used for each day analysed. All data for a given day were employed but not all stations were recording on all days. If a station was recording on a particular day then it recorded for the whole 24 hours of that day.

Figs. 5 - 14 show the results of these analyses. In each case the "a" part of the figure shows the results from the turbulence model presented here. The "b" part of the figure shows the results from the Gradient Drift Instability model presented in [*Burston et al.*, 2009]. Only the correlation co-efficients with p-values < 5% are plotted. The vertical error bars are ± 20km, representing the height range of a voxel. The horizontal error bars represent the 95% confidence limits for the correlation co-

efficients. Results for all assumed altitudes of ionospheric pierce point (IPP) are shown. No results are available at altitudes greater than 500km because no ray-paths from GPS satellites to scintillation receivers go through voxels at such altitudes. This is because the elevation angles between the satellites and receivers are low. Because all the ray paths have low elevation angles, none is parallel or close to parallel to the magnetic field direction, which will be almost vertical in the region under consideration. This means that the model is not affected by any elongation of irregularities parallel to the magnetic field which might exist. Plots for S_4 and σ_ϕ(3s) correlations for each storm period are presented (figs 5-12). If no results appear at a given altitude then no correlation co-efficients with p-values < 5% were found during that storm period at that assumed IPP altitude. There are no σ_ϕ(3s) correlation co-efficients with p-value < 5% for October 30th 2003 or May 14-16th 2005 so σ_ϕ(10s) results are shown instead (figs 6 and 12). The results for σ_ϕ over mean time intervals longer than those shown in the graphs are similar to those in the figures.

Figs.13-14 show the same results collating all analysed days on to one graph each for S_4 and σ_ϕ(3s) correlations. When interpreting the graphs in figs.5-14 the most important factor is whether or not, at any given altitude, there are positive or negative values and how many of each. Positive correlations without negative correlations at a given altitude make a case for the turbulence process occurring and vice versa. When positive and negative correlations appear at a given altitude the interpretation is more ambiguous, depending on how many of each there are, their exact values and confidence ranges as shown by the error bars.

Conclusions

Figs.13-14, the results for all days analysed, show an overall picture of little correlation between the modelled mean turbulent wave amplitude and the scintillation indices S_4 and σ_ϕ. For the GDI case, they show stronger correlation, particularly when the chosen ionospheric pierce points are at plausible ionospheric altitudes (200-440km).

Looking in more detail at individual storm periods the situation revealed is not so straightforward. Comparison of the turbulence case with the GDI case shows two storms, July and November 2004, where results suggest approximately equal evidence of correlation between the mean wave amplitudes and the S_4 observations. In the July 2004 case the σ_ϕ(3s) results also look approximately equally positive for correlations with each mechanism. The other two storms analysed (October 30th 2003 and May 2005) show the GDI mechanism as correlating better than the turbulence mechanism.

In summary, the turbulence process of plasma irregularity generation sometimes correlates with observed scintillation indices approximately as well as the GDI process.

These results do not, however, indicate one way or the other, which process is dominating the formation of irregularities over a given time or volume of ionosphere, except where the GDI process has significant positive correlation and the turbulence process has not, or vice versa. The linear correlation co-efficient takes no account of

the difference in absolute size of the results contained in the two data sets, modelled mean wave amplitude due to the GDI process and modelled mean wave amplitude due to the turbulence process. It is possible that whilst equally well correlated with the scintillation observations, the mean amplitudes from the GDI model are always larger than the equivalent mean amplitudes for the turbulence process, or vice versa. In such circumstances the process with consistently larger mean wave amplitudes would dominate the process of irregularity formation in plasma patches. It should be re-iterated here, that the results anyway show better correlation with the GDI process when considering all the days analysed as a whole.

Each calculation of γ_T made by this model relies on a value for the constant, β, calculated from data presented in [*Mounir et al.*, 1991]. It is used because it is the only value that could be obtained (see fig.4.1.). However, if assumed constant, any value of β used will not affect the correlation co-efficients presented here. Although it is likely that β will in reality vary across time and space, theoretical knowledge of the distribution of values is absent. It is therefore possible that using a range of values for β could introduce greater inaccuracy, as the correlation co-efficients would then be affected by the arbitrary choice of range and distribution made. Better knowledge of the turbulent spectrum of the polar-cap electric field would aid this model tremendously by allowing more accurate calculations of γ_T.

The conclusion drawn from the analyses presented here, that turbulence might in some circumstances be of equal significance to the GDI process in determining the way irregularities form in polar cap plasma patches, shows a need for further study of

turbulence in plasma patches, since it has not been as thoroughly investigated as the GDI process.

References

Burston, R., et al. (2009), Correlation between scintillation indices and gradient drift wave amplitudes in the northern polar ionosphere, *Journal of Geophysical Research-Space Physics*, *114*.

Chaturvedi, P. K., and S. L. Ossakow (1979), Non-Linear Stabilization of the Current Convective Instability in the Diffuse Aurora, *Geophysical Research Letters*, *6*(12), 957-959.

Chaturvedi, P. K., and S. L. Ossakow (1981), The Current Convective Instability as Applied to the Auroral Ionosphere, *Journal of Geophysical Research-Space Physics*, *86*(NA6), 4811-4814.

Chaturvedi, P. K., et al. (1994), Effects of Field Line Mapping on the Gradient-Drift Instability in the Coupled E-Region and F-Region High-Latitude Ionosphere, *Radio Science*, *29*(1), 317-335.

Coley, W. R., and R. A. Heelis (1995), Adaptive Identification and Characterization of Polar Ionization Patches, *Journal of Geophysical Research-Space Physics*, *100*(A12), 23819-23827.

Davies, K. (1990), *Ionospheric Radio*, Peter Peregrinus, London.

Gondarenko, N. A., and P. N. Guzdar (1999), Gradient drift instability in high latitude plasma patches: ion inertial effects, *Geophysical Research Letters*, *26*(22), 3345-3348.

Gondarenko, N. A., and P. N. Guzdar (2001), Three-dimensional structuring characteristics of high-latitude plasma patches, *Journal of Geophysical Research-Space Physics*, *106*(A11), 24611-24620.

Gondarenko, N. A., et al. (2003), Structuring of high latitude plasma patches with variable drive, *Geophysical Research Letters*, *30*(4).

Gondarenko, N. A., and P. N. Guzdar (2004a), Plasma patch structuring by the nonlinear evolution of the gradient drift instability in the high-latitude ionosphere, *Journal of Geophysical Research-Space Physics*, *109*(A9).

Gondarenko, N. A., and P. N. Guzdar (2004b), Density and electric field fluctuations associated with the gradient drift instability in the high-latitude ionosphere, *Geophysical Research Letters*, *31*(11).

Gondarenko, N. A., et al. (2005), Generation and evolution of density irregularities due to self-focusing in ionospheric modifications, *Journal of Geophysical Research-Space Physics*, *110*(A9).

Gondarenko, N. A. a. P. N. G. (2006a), Nonlinear three-dimensional simulations of mesoscale structuring by multiple drives in high-latitude plasma patches, *Journal of Geophysical Research-Space Physics*, *111*(A8).

Gondarenko, N. A. a. P. N. G. (2006b), Simulations of the scintillation-producing irregularities in high-latitude plasma patches, *Geophysical Research Letters*, *33*(22).

H. Mounir, J. C. C., A. Berthelier, D. Lagoutte and C. Beghin (1991), The Small-scale turbulent structure of the high latitude ionosphere: ARCAD-AUREOL-3 observations, *Annales Geophysicae*, *9*, 725-737.

Hargreaves, J. K. (1992), *The Solar-Terrestrial Environment*, Cambridge University Press.

Huba, J. D. (1984), Long Wavelength Limit of the Current Convective Instability, *Journal of Geophysical Research-Space Physics*, *89*(NA5), 2931-2935.

Huba, J. D., et al. (1985), Ionospheric Turbulence - Interchange Instabilities and Chaotic Fluid Behavior, *Geophysical Research Letters*, *12*(1), 65-68.

Hunsucker, R. D. a. J. K. H. (2003), *The High-Latitude Ionosphere and its Effects on Radio Propagation*, 1 ed., 617 pp., Cambridge University Press, Cambridge.

Kaplan, E. D. e. (1996), *Understanding GPS: Principles and Applications.*, Artech House Publishers, Boston.

Kelley, M. C. (1989), *The Earth's Ionosphere: Plasma Physics and Electrodynamics*, 1 ed., Academic Press.

Kelley, M. C. (2009), *The Earth's Ionosphere: Plasma Physics and Electrodynamics*, 2 ed.

Kersley, L., et al. (1989), Scintillation and Eiscat Investigations of Gradient-Drift Irregularities in the High-Latitude Ionosphere, *Journal of Atmospheric and Terrestrial Physics*, *51*(4), 241-247.

Kintner, P. M., and C. E. Seyler (1985), The Status of Observations and Theory of High-Latitude Ionospheric and Magnetospheric Plasma Turbulence, *Space Science Reviews*, *41*(1-2), 91-129.

Kivanc, O., and R. A. Heelis (1997), Structures in ionospheric number density and velocity associated with polar cap ionization

patches, *Journal of Geophysical Research-Space Physics*, *102*(A1), 307-318.

Kunitsyn, V. E., and E. D. Tereshchenko (1992), Determination of the Turbulent Spectrum in the Ionosphere by a Tomographic Method, *Journal of Atmospheric and Terrestrial Physics*, *54*(10), 1275-1282.

Macmillan, S., and S. Maus (2005), International geomagnetic reference field - the tenth generation, *Earth Planets and Space*, *57*(12), 1135-1140.

Maus, S., et al. (2005a), The 10th generation international geomagnetic reference field, *Physics of the Earth and Planetary Interiors*, *151*(3-4), 320-322.

Maus, S., et al. (2005b), The 10th-Generation International Geomagnetic Reference Field, *Geophysical Journal International*, *161*(3), 561-565.

Maus, S., et al. (2005c), NGDC/GFZ candidate models for the 10th generation International Geomagnetic Reference Field, *Earth Planets and Space*, *57*(12), 1151-1156.

Mounir, H., et al. (1991), The Small-Scale Turbulent Structure of the High-Latitude Ionosphere - Arcad-Aureol-3 Observations, *Annales Geophysicae-Atmospheres Hydrospheres and Space Sciences*, *9*(11), 725-737.

Ossakow, S. L., and P. K. Chaturvedi (1979), Current Convective Instability in the Diffuse Aurora, *Geophysical Research Letters*, *6*(4), 332-334.

Sojka, J. J., et al. (1998), Gradient drift instability growth rates from global-scale modeling of the polar ionosphere, *Radio Science*, *33*(6), 1915-1928.

Spencer, P. S. J., and C. N. Mitchell (2007), Imaging of fast moving electron-density structures in the polar cap, *Annals of Geophysics*, *50*(3), 427-434.

Zvezdin, V. N., and S. V. Fridman (1992), Regimes of Ionospheric Turbulence from Fractal Analysis of Satellite Radio Signal Scintillations, *Journal of Atmospheric and Terrestrial Physics*, *54*(7-8), 957-962.

Figure Captions

Fig.1: A tomographic reconstruction of the northern polar-cap ionosphere, created by MIDAS 2.0 and showing plasma patches. Weimer Model predictions of $\mathbf{E} \times \mathbf{B}$ drifts are shown by arrows.

Fig. 2a: All sky camera image for 22.00 UT, 30th October, 2003. The camera is located at Qaanaaq, Greenland (77.47º N, 69.27º W). 630nm wavelengthlight is recorded. The dark triangle is the shadow of an ionosonde mast, obscuring part of the field of view. Note that the image has been rotated to the same orientation as in fig.3b.

Fig.2b: MIDAS 2.0 reconstruction using a 2ºx4º latitude x longitude grid. The comparison between figs.4a and 4b is typical of that obtainable by MIDAS 2.0. The location of the All Sky Camera is marked by the asterisk.

Fig.3: Locations of GPS Scintillation Receiver Stations used in this Study.

Fig.4: Sketch showing how the constant, β, is calculated from a power spectral density graph.

Fig.5a: Correlation of S4 with Modelled Mean Turbulent Wave Amplitude (May 2005 storm).

Fig.5b: Correlation of S4 with Modelled Mean Gradient Drift Wave Amplitude (May 2005 storm).

Fig.6a: Correlation of σ_ϕ(10s) with Modelled Mean Turbulent Wave Amplitude (May 2005 storm).

Fig.6b: Correlation of σ_ϕ(10s) with Modelled Mean Gradient Drift Wave Amplitude (May 2005 storm).

Fig.7a: Correlation of S4 with Modelled Mean Turbulent Wave Amplitude (November 2004 storm).

Fig.7b: Correlation of S4 with Modelled Mean Gradient Drift Wave Amplitude (November 2004 storm).

Fig.8a: Correlation of σ_ϕ(3s) with Modelled Mean Turbulent Wave Amplitude (November 2004 storm).

Fig.8b: Correlation of σ_ϕ(3s) with Modelled Mean Gradient Drift Wave Amplitude (November 2004 storm).

Fig.9a: Correlation of S4 with Modelled Mean Turbulent Wave Amplitude (July 2004 storm).

Fig. 9b: Correlation of S4 with Modelled Mean Gradient Drift Wave Amplitude (July 2004 storm).

Fig.10a: Correlation of σ_ϕ(3s) with Modelled Mean Turbulent Wave Amplitude (July 2004 storm).

Fig.10b: Correlation of σ_ϕ(3s) with Modelled Mean Gradient Drift Wave Amplitude (November 2004 storm).

Fig.11a: Correlation of S4 with Modelled Mean Turbulent Wave Amplitude (October 30th 2003 storm).

Fig.11b: Correlation of S4 with Modelled Mean Gradient Drift Wave Amplitude (October 30th 2003 storm).

Fig.12a: Correlation of σ_ϕ(10s) with Modelled Mean Turbulent Wave Amplitude (October 30th 2003 storm).

Fig.12b: Correlation of σ_ϕ(10s) with Modelled Mean Gradient Drift Wave Amplitude (October 30th 2003 storm).

Fig.13a: Correlation of S4 with Modelled Mean Turbulent Wave Amplitude (All Days).

Fig.13b: Correlation of S4 with Modelled Mean Gradient Drift Wave Amplitude (All Days).

Fig.14a: Correlation of σ_ϕ(3s) with Modelled Mean Gradient Drift Wave Amplitude (All Days).

Fig.14b: Correlation of σ_ϕ(3s) with Modelled Mean Gradient Drift Wave Amplitude (All Days).

Tables

Dates of Storms Used in this Analysis

Storm 1	Storm 2	Storm 3	Storm 4
30th Oct 2003	24-28th July 2004	8-11th Nov 2004	14-16th May 2005

Table 1: Dates of Storms analysed in this study.

Locations of GPS Scintillation Receivers Used

Station Name	Latitude (Geographic)	Longitude (Geographic)
Athabasca	54.7ºN	113.3ºW
Calgary	51.1°N	114.1°W
Kiruna	67.9ºN	20.4ºE
Sodankyla	67.4ºN	26.6ºE
Svarlbard	78.9ºN	11.9ºE
Tromso	69.6º N	19.2ºE
Yellowknife	62.5°N	114.5ºW

Table 2: Locations of GPS scintillation receivers, data from which are used in this study.

	Station	
	Athabasca	Calgary
30th	√	

	Station	
	Athabasca	Calgary
24th		
25th		
26th		
27th		
28th		

	Station	
	Athabasca	Calgary
8th		
9th		
10th		
11th		

	Station	
	Athabasca	Calgary
14th		✓
15th		✓
16th		✓

Table 3: Scintillation receiver stations used for each day analysed.

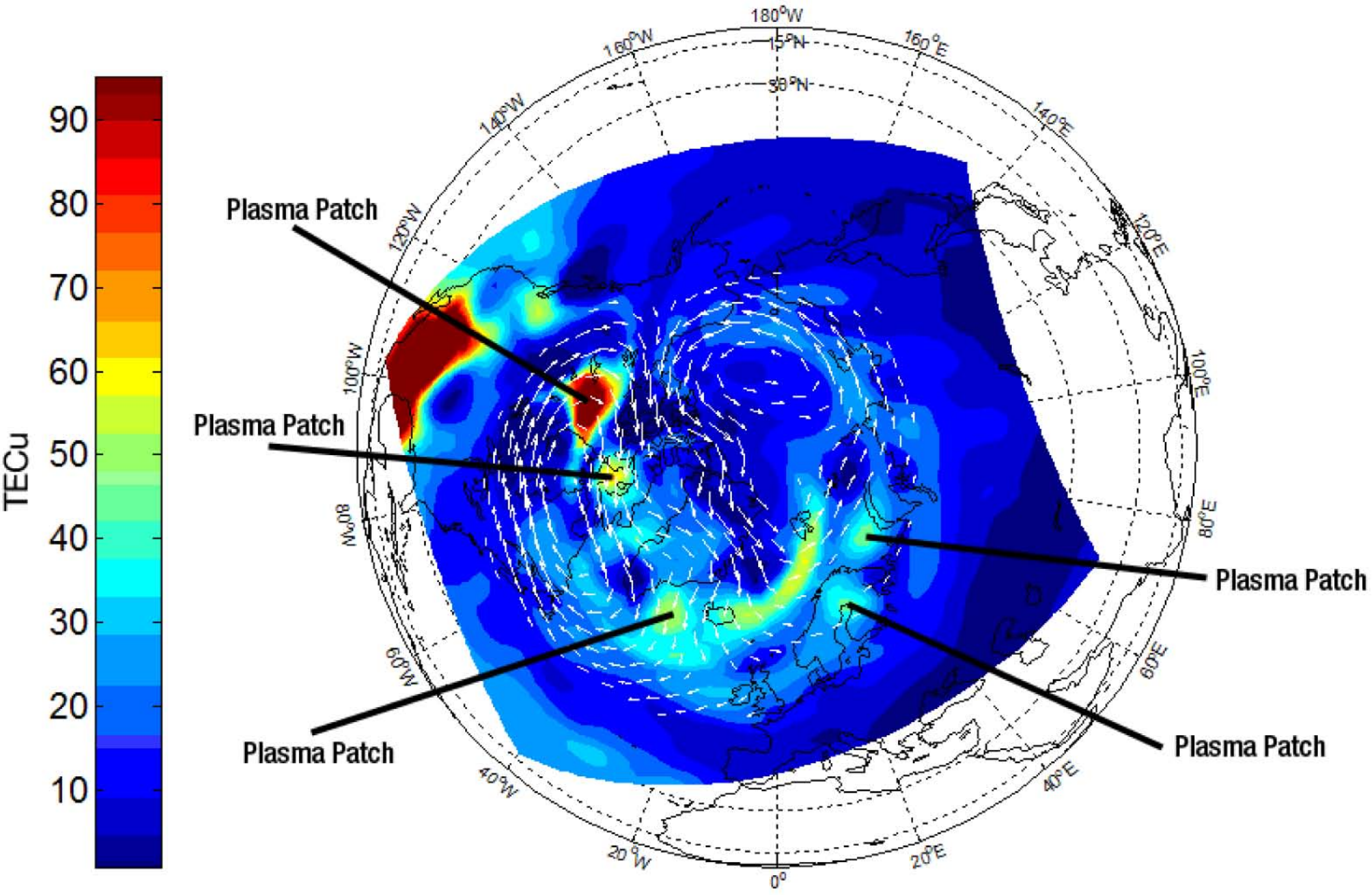

Total Electron Content 30-Oct-2003 21:40:00UT

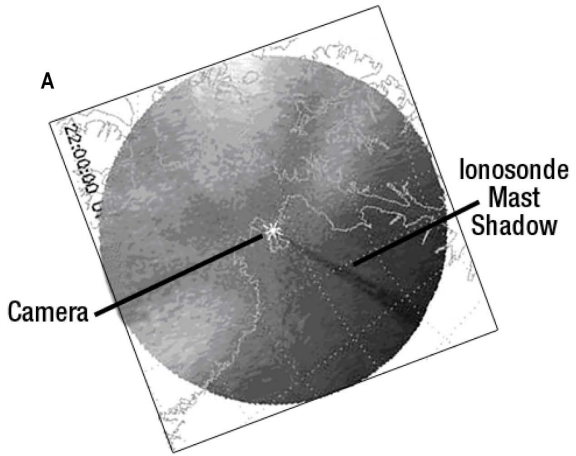

22:00:00 UT 30th Oct 2003

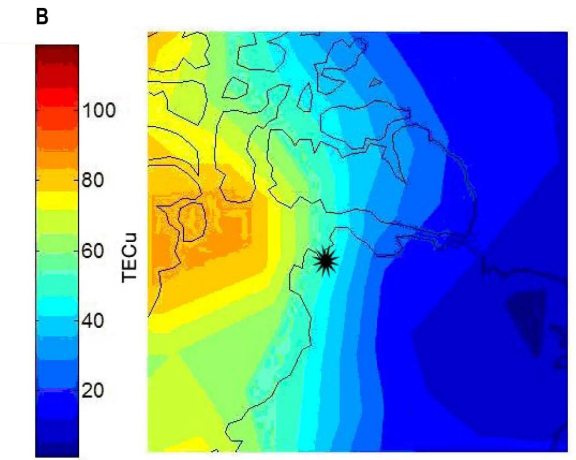

Total Electron Content 30-Oct-2003 22:00:00UT


N 09
75° N
N 06
Calgary
Athabasca
Yellowknife
Ny Alesund
Tromso
Sodankyla
Kiruna

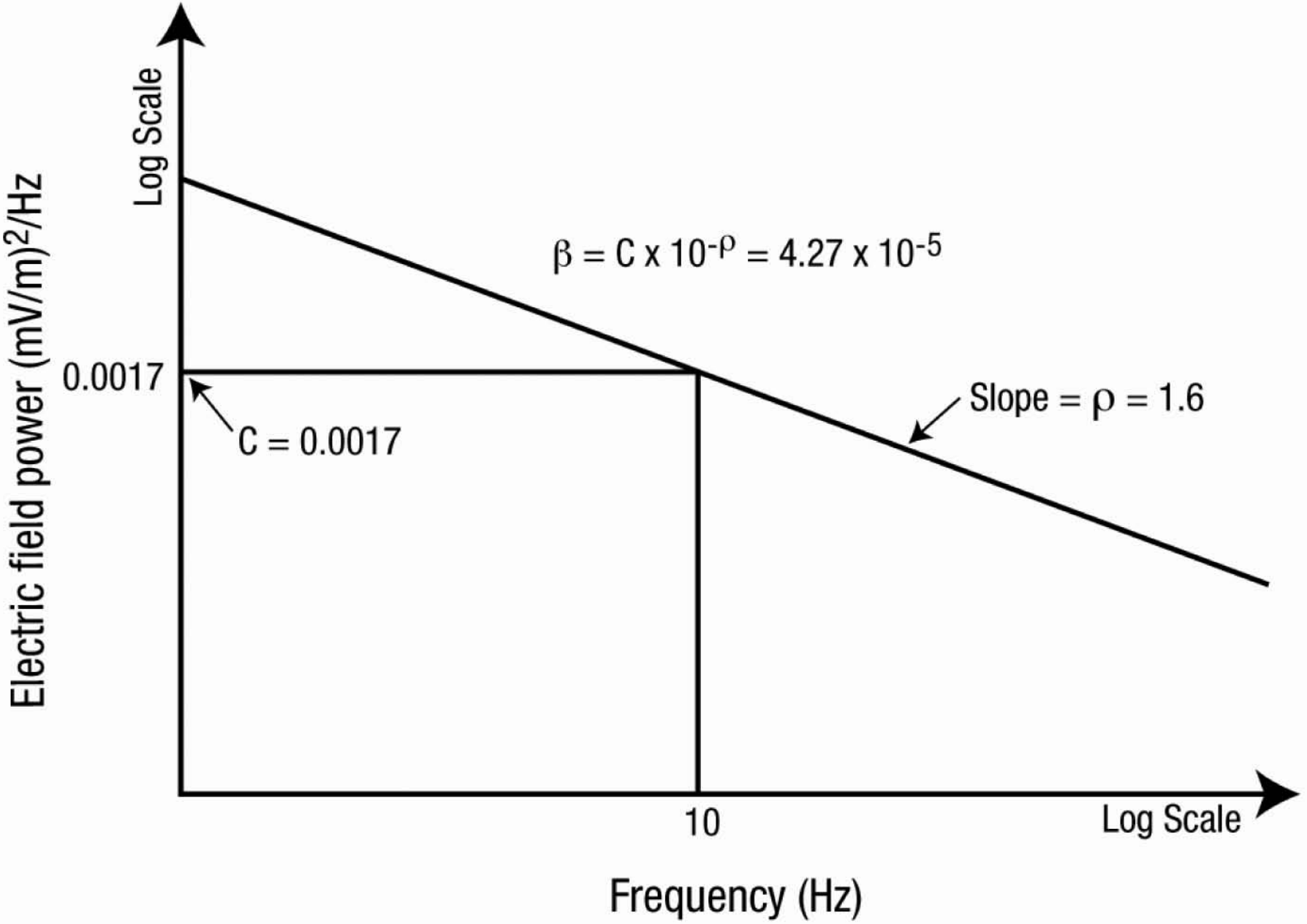
Log Scale
Electric field power (mV/m)²/Hz
β = C x 10^-ρ = 4.27 x 10^-5
0.0017
C = 0.0017
Slope = ρ = 1.6
10
Log Scale
Frequency (Hz)

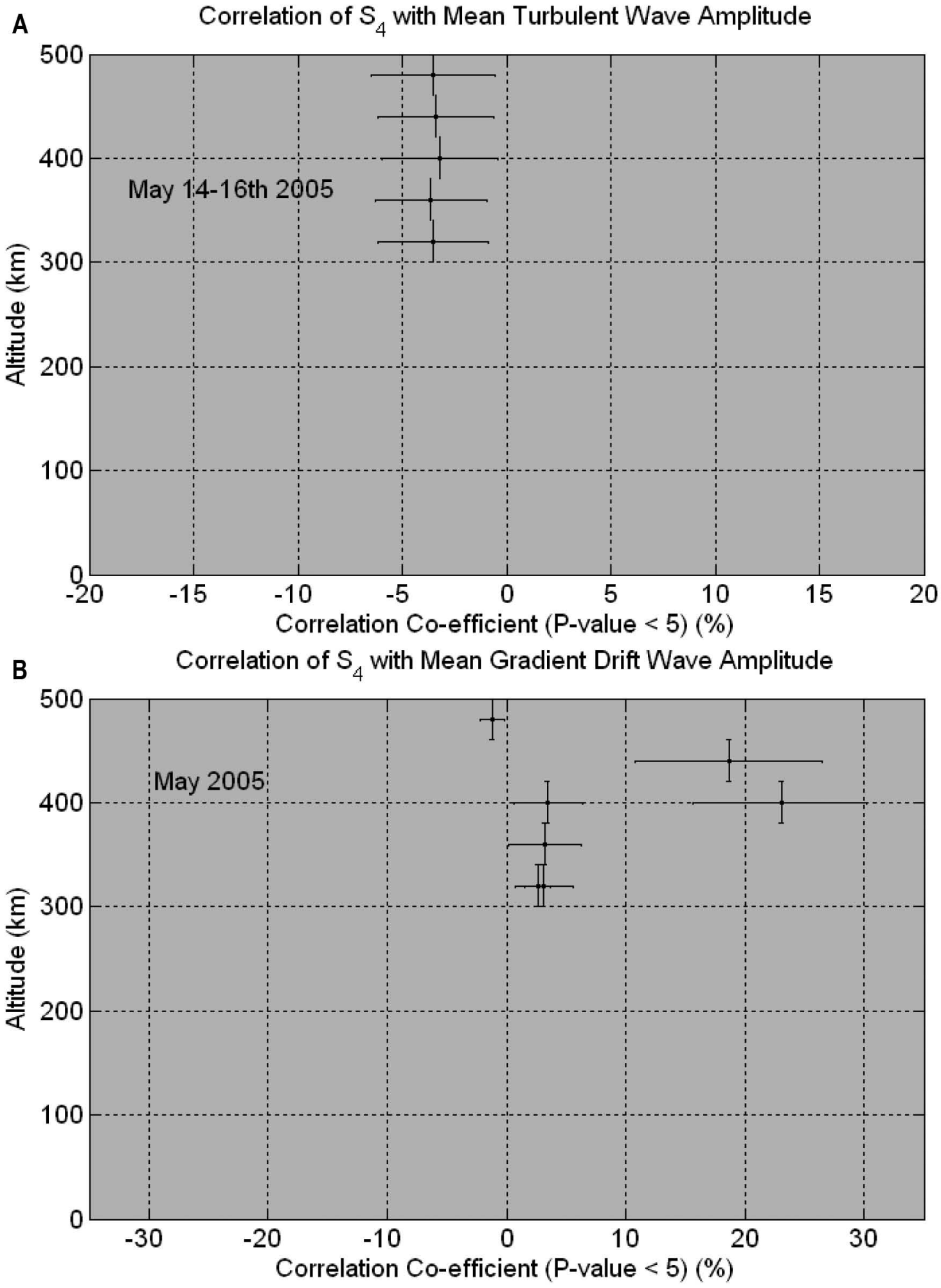
A
Correlation of S_4 with Mean Turbulent Wave Amplitude
May 14-16th 2005
Altitude (km)
500
400
300
200
100
0
-20
-15
-10
-5
0
5
10
15
20
Correlation Co-efficient (P-value < 5) (%)
B
Correlation of S_4 with Mean Gradient Drift Wave Amplitude
May 2005
Altitude (km)
500
400
300
200
100
0
-30
-20
-10
0
10
20
30
Correlation Co-efficient (P-value < 5) (%)

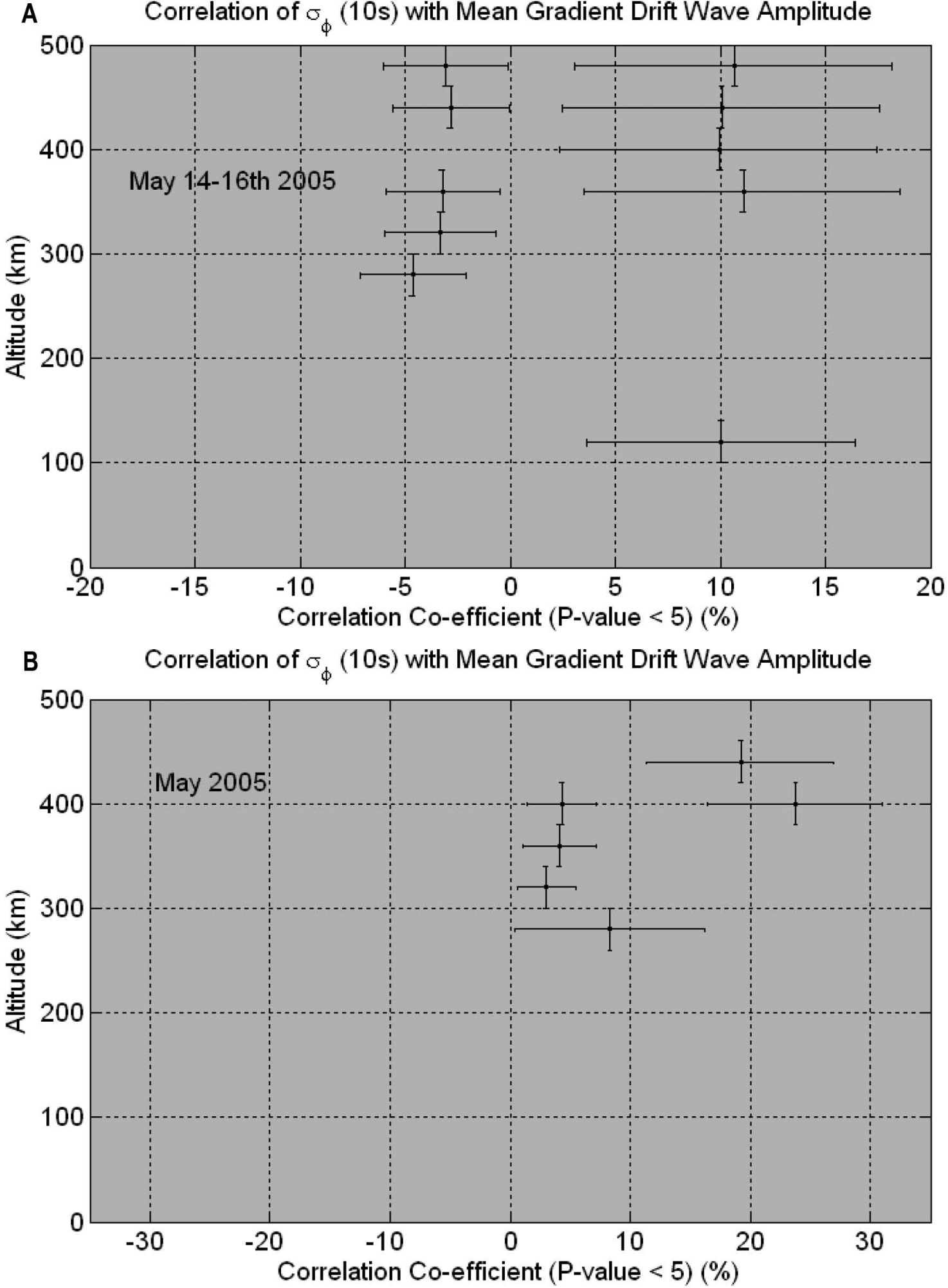
A
Correlation of σ_ϕ (10s) with Mean Gradient Drift Wave Amplitude
May 14-16th 2005
Altitude (km)
Correlation Co-efficient (P-value < 5) (%)
B
Correlation of σ_ϕ (10s) with Mean Gradient Drift Wave Amplitude
May 2005
Altitude (km)
Correlation Co-efficient (P-value < 5) (%)

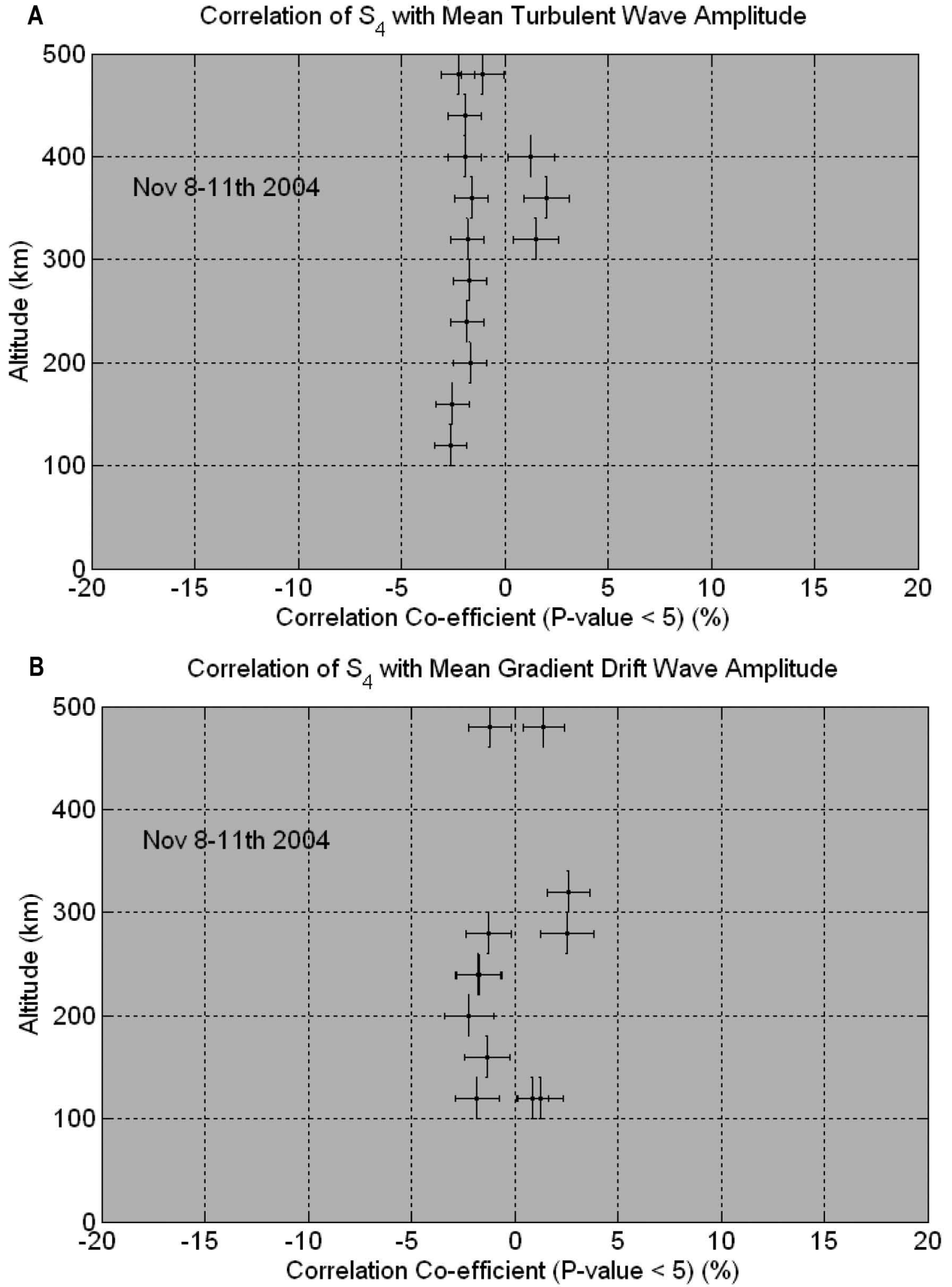
A
Correlation of S_4 with Mean Turbulent Wave Amplitude
Nov 8-11th 2004
Altitude (km)
500
400
300
200
100
0
-20
-15
-10
-5
0
5
10
15
20
Correlation Co-efficient (P-value < 5) (%)
B
Correlation of S_4 with Mean Gradient Drift Wave Amplitude
Nov 8-11th 2004
Altitude (km)
500
400
300
200
100
0
-20
-15
-10
-5
0
5
10
15
20
Correlation Co-efficient (P-value < 5) (%)

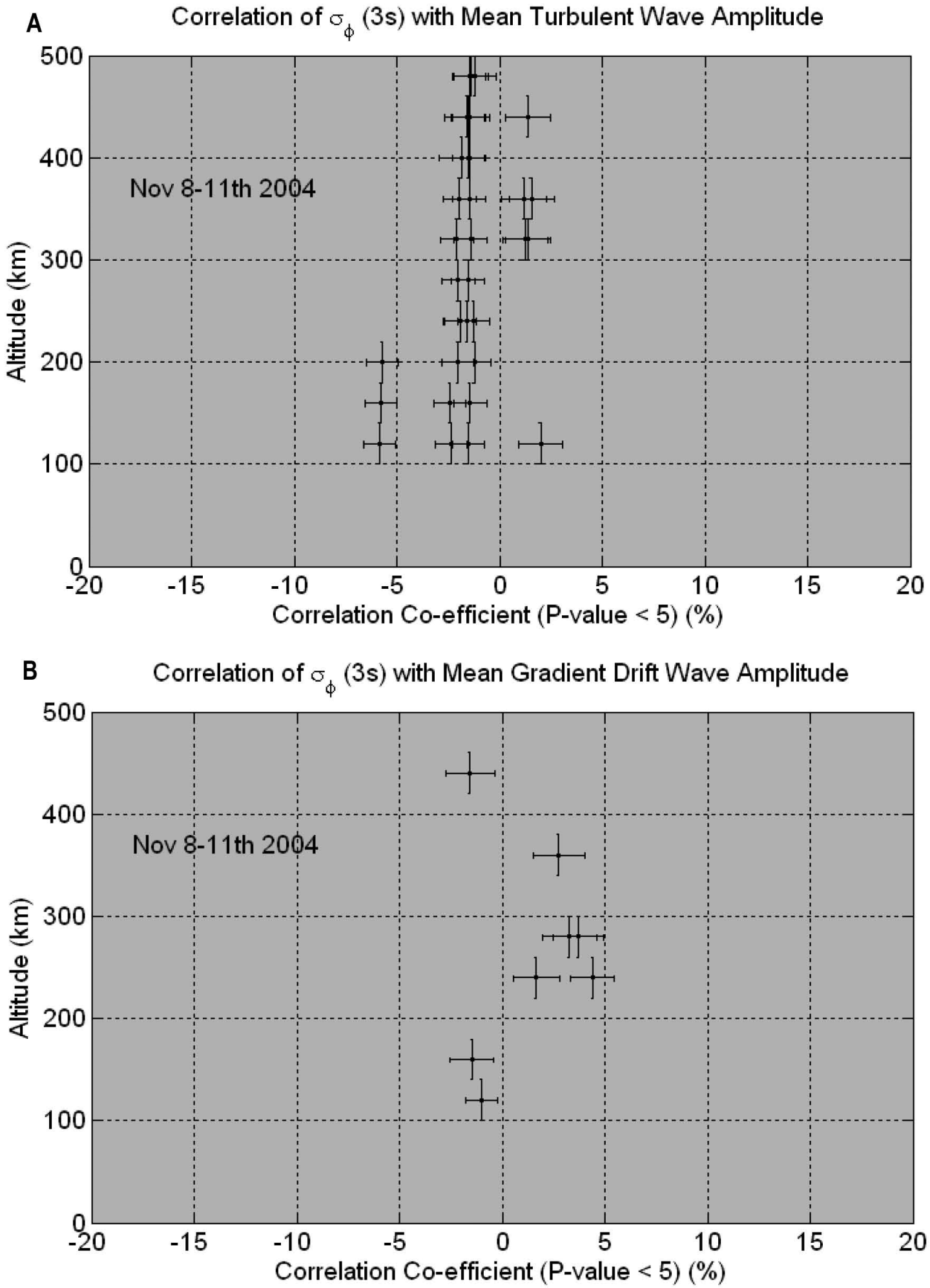
A
Correlation of σ_ϕ (3s) with Mean Turbulent Wave Amplitude
Nov 8-11th 2004
Altitude (km)
Correlation Co-efficient (P-value < 5) (%)
B
Correlation of σ_ϕ (3s) with Mean Gradient Drift Wave Amplitude
Nov 8-11th 2004
Altitude (km)
Correlation Co-efficient (P-value < 5) (%)

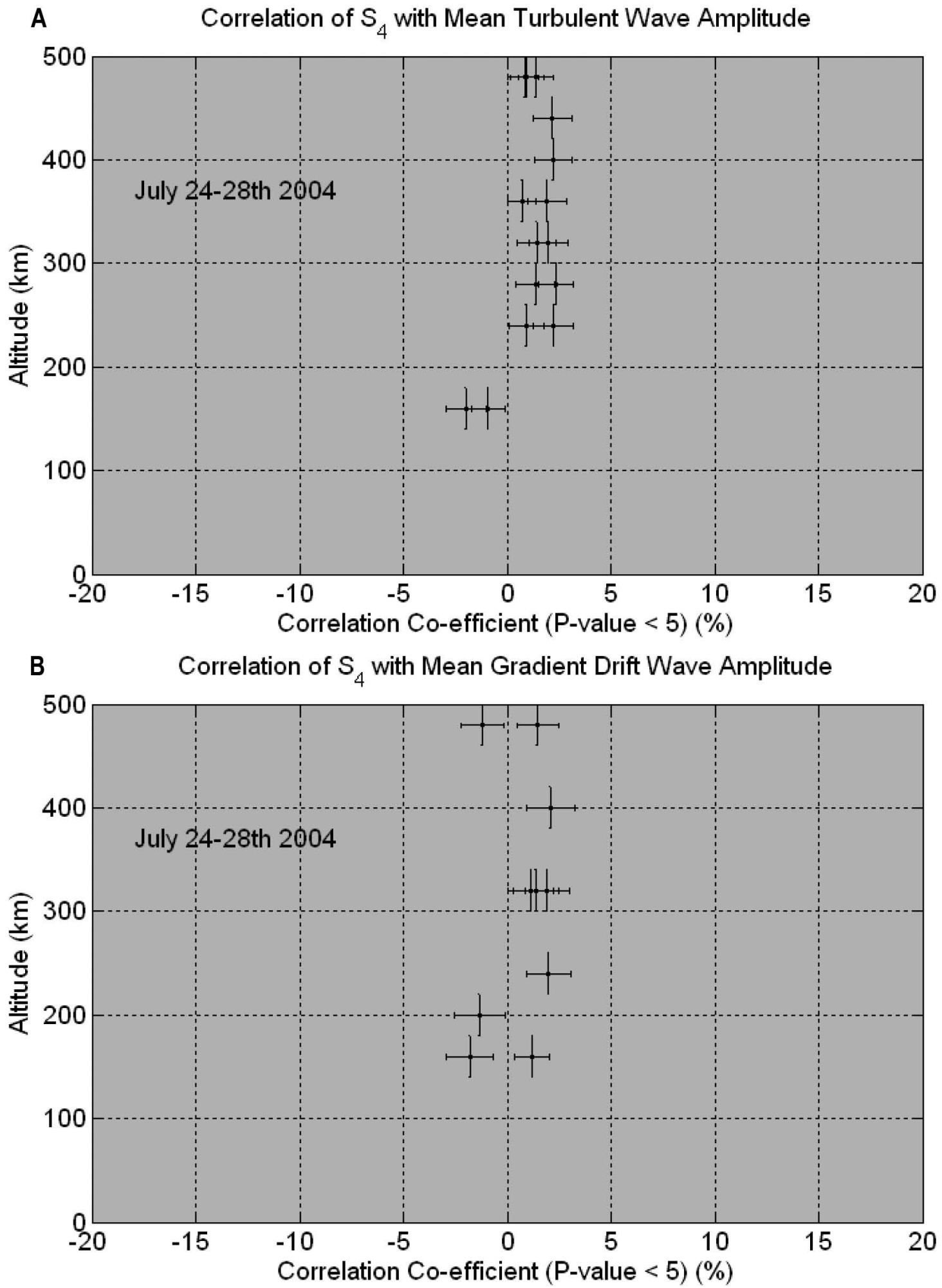
A
Correlation of S_4 with Mean Turbulent Wave Amplitude
July 24-28th 2004
Altitude (km)
Correlation Co-efficient (P-value < 5) (%)
B
Correlation of S_4 with Mean Gradient Drift Wave Amplitude
July 24-28th 2004
Altitude (km)
Correlation Co-efficient (P-value < 5) (%)

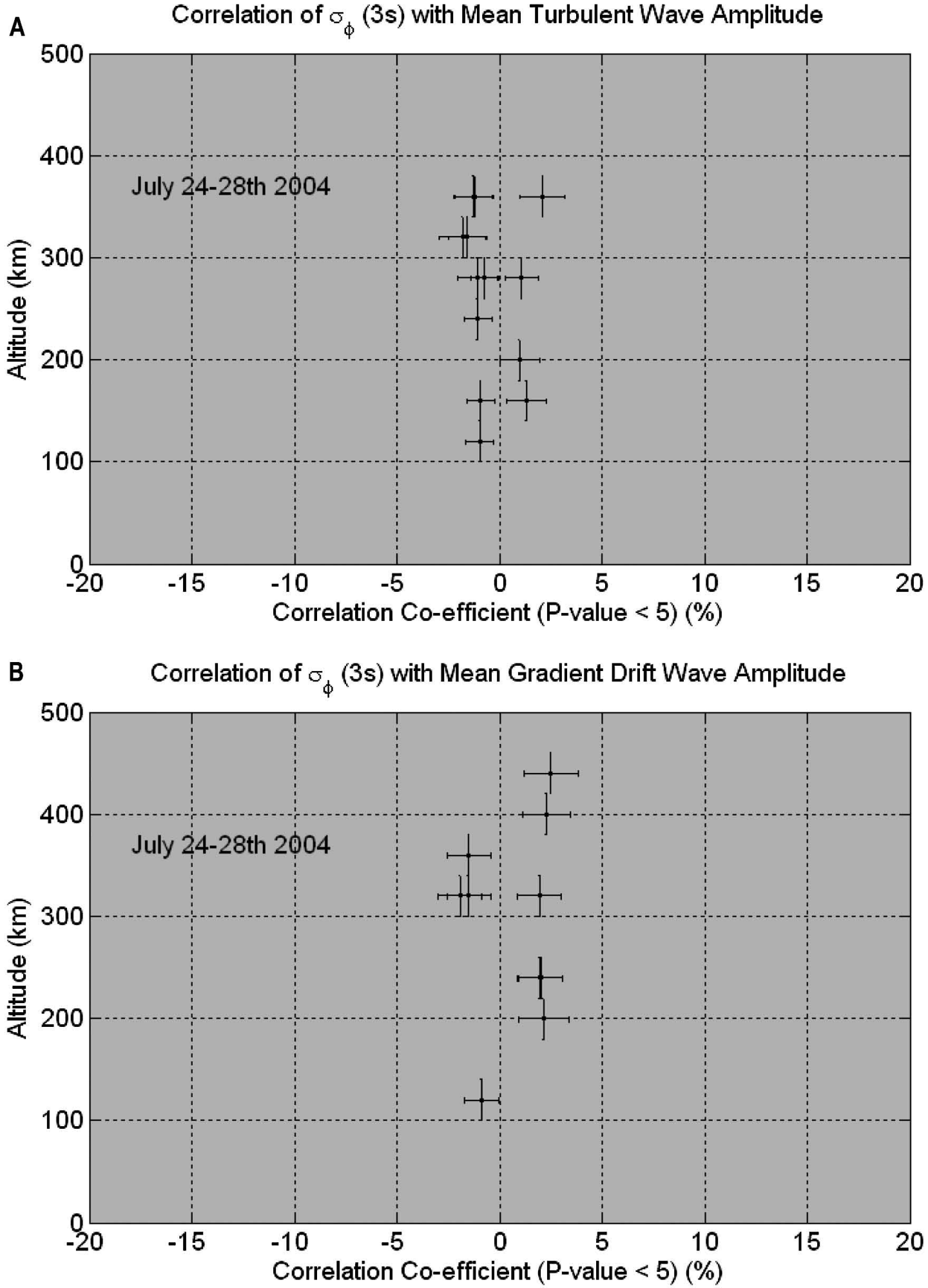
A
Correlation of σ_ϕ (3s) with Mean Turbulent Wave Amplitude
July 24-28th 2004
Altitude (km)
Correlation Co-efficient (P-value < 5) (%)
B
Correlation of σ_ϕ (3s) with Mean Gradient Drift Wave Amplitude
July 24-28th 2004
Altitude (km)
Correlation Co-efficient (P-value < 5) (%)

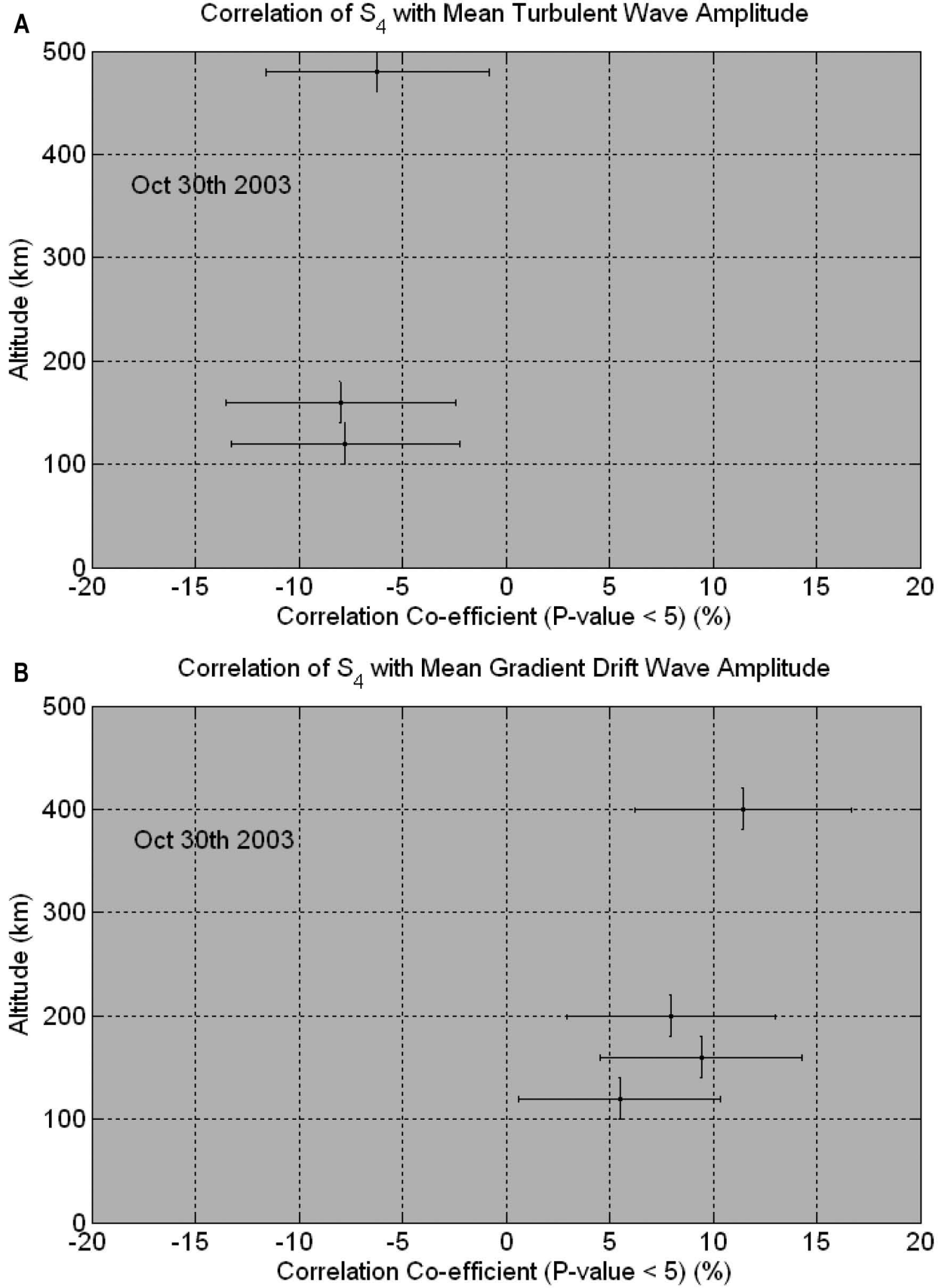
A
Correlation of S_4 with Mean Turbulent Wave Amplitude
Oct 30th 2003
Altitude (km)
500
400
300
200
100
0
-20
-15
-10
-5
0
5
10
15
20
Correlation Co-efficient (P-value < 5) (%)
B
Correlation of S_4 with Mean Gradient Drift Wave Amplitude
Oct 30th 2003
Altitude (km)
500
400
300
200
100
0
-20
-15
-10
-5
0
5
10
15
20
Correlation Co-efficient (P-value < 5) (%)

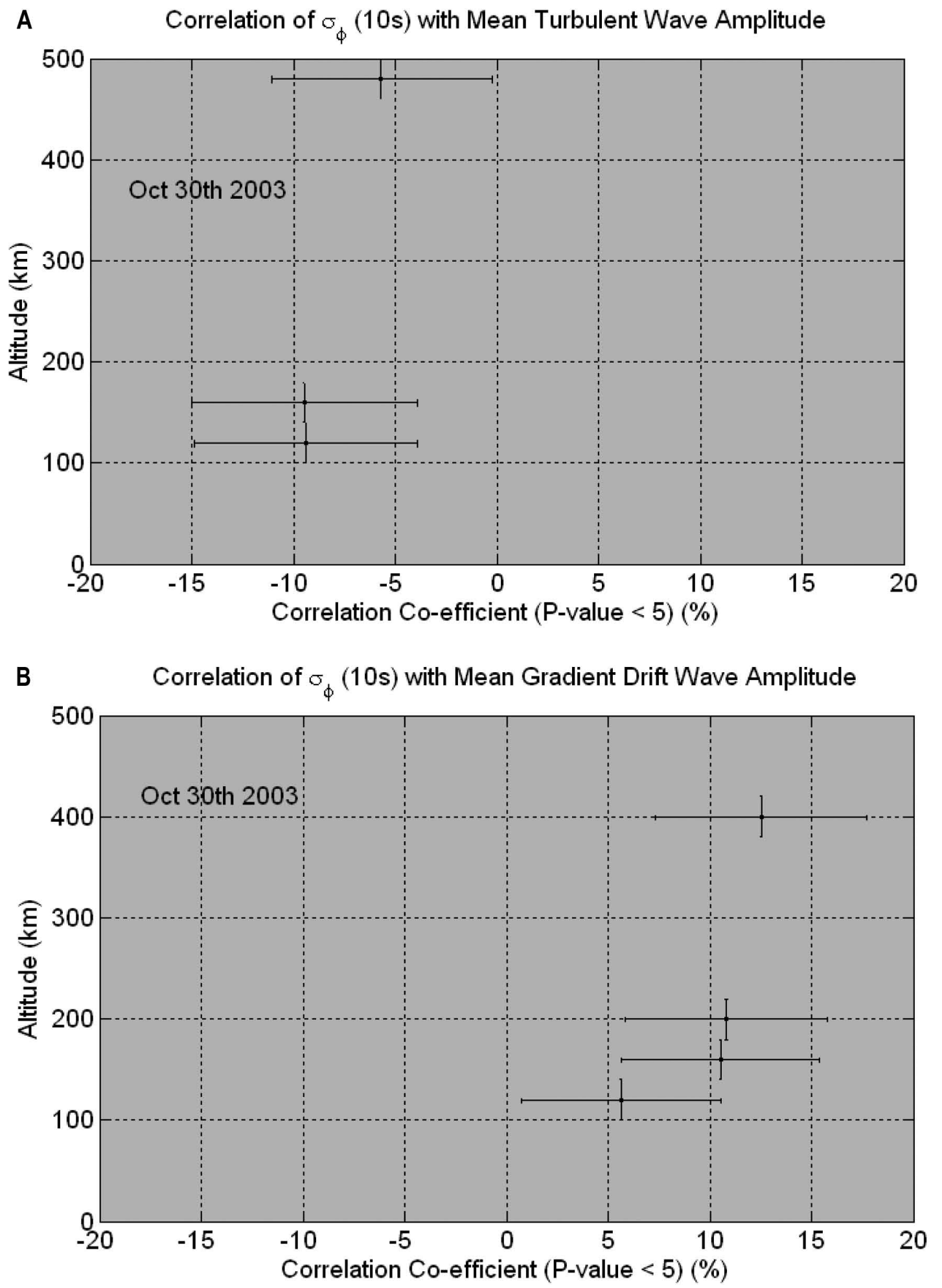
A
Correlation of σφ (10s) with Mean Turbulent Wave Amplitude
Oct 30th 2003
Altitude (km)
Correlation Co-efficient (P-value < 5) (%)
B
Correlation of σφ (10s) with Mean Gradient Drift Wave Amplitude
Oct 30th 2003
Altitude (km)
Correlation Co-efficient (P-value < 5) (%)

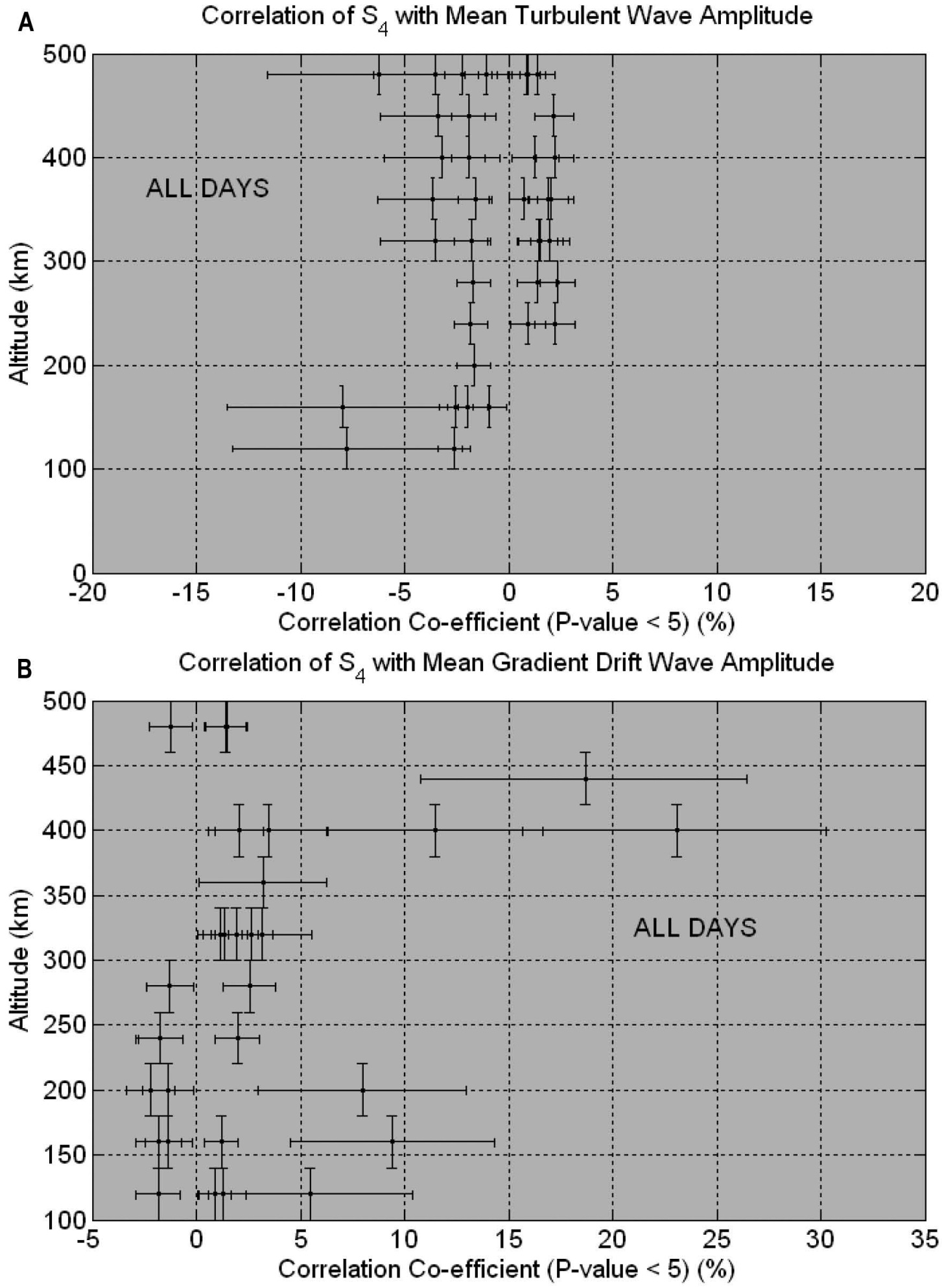
A
Correlation of S_4 with Mean Turbulent Wave Amplitude
ALL DAYS
Altitude (km)
500
400
300
200
100
0
-20
-15
-10
-5
0
5
10
15
20
Correlation Co-efficient (P-value < 5) (%)
B
Correlation of S_4 with Mean Gradient Drift Wave Amplitude
ALL DAYS
Altitude (km)
500
450
400
350
300
250
200
150
100
-5
0
5
10
15
20
25
30
35
Correlation Co-efficient (P-value < 5) (%)

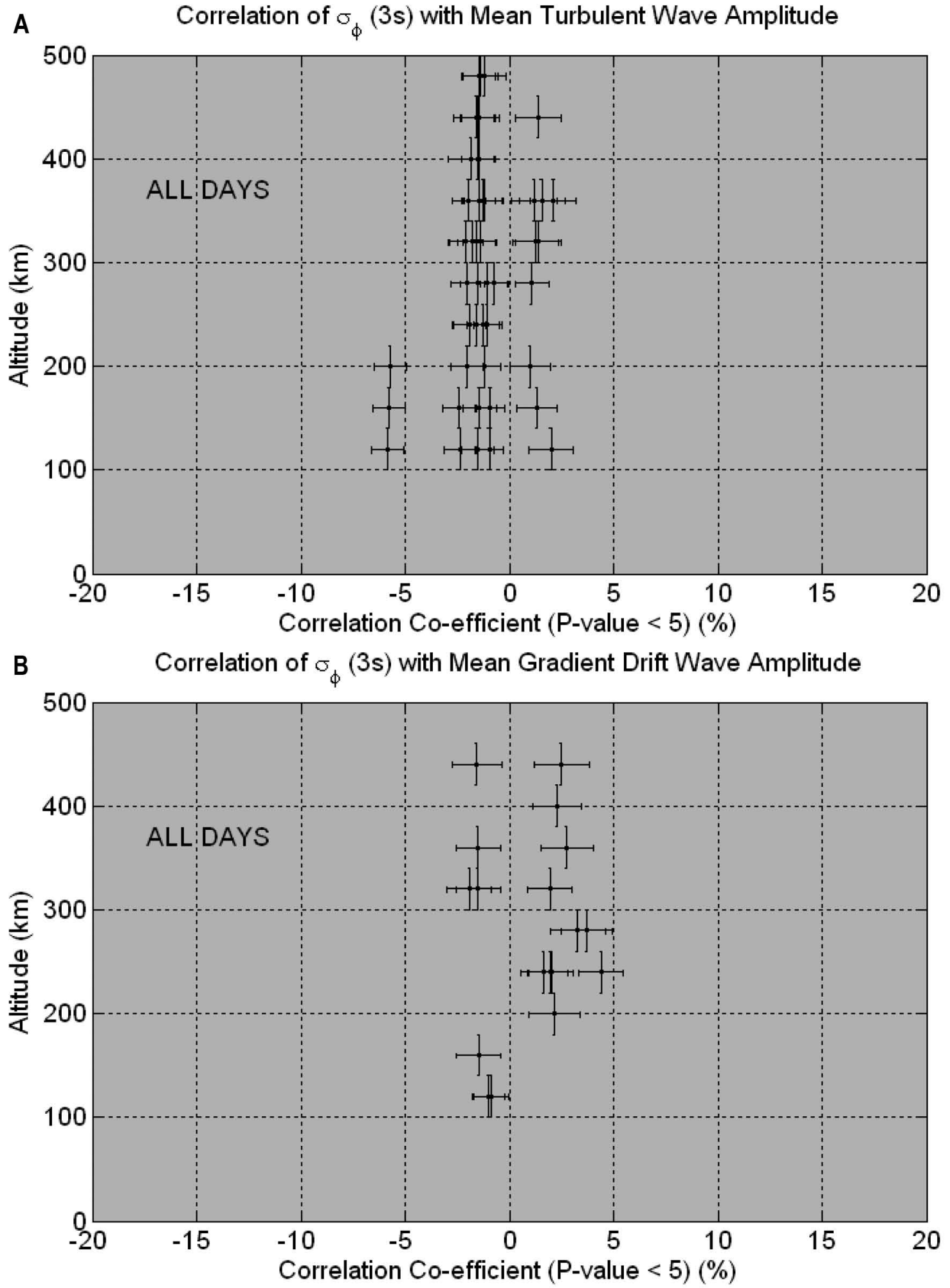
A
Correlation of σ_ϕ (3s) with Mean Turbulent Wave Amplitude
ALL DAYS
Altitude (km)
500
400
300
200
100
0
-20
-15
-10
-5
0
5
10
15
20
Correlation Co-efficient (P-value < 5) (%)
B
Correlation of σ_ϕ (3s) with Mean Gradient Drift Wave Amplitude
ALL DAYS
Altitude (km)
500
400
300
200
100
0
-20
-15
-10
-5
0
5
10
15
20
Correlation Co-efficient (P-value < 5) (%)